electronic reprint

Journal of
Applied Crystallography
ISSN 0021-8898

A comparative study of single-line and Rietveld strain–size evaluation procedures using MgO ceramics

Suminar Pratapa, Brian O'Connor and Brett Hunter

Journal of
Applied Crystallography
ISSN 0021-8898

Received 4 June 2001
Accepted 29 November 2001

A comparative study of single-line and Rietveld strain–size evaluation procedures using MgO ceramics

Suminar Pratapa,[a]*† Brian O'Connor[a] and Brett Hunter[b]

[a]Materials Research Group, Department of Applied Physics, Curtin University of Technology, Perth, Australia, and [b]Australian Nuclear Science and Technology Organization, Lucas Heights Research Laboratories, Menai, New South Wales, Australia. Correspondence e-mail: pratapas@ses.curtin.edu.au

Strain–size evaluations from diffraction line broadening for MgO ceramic materials have been compared using single-line integral-breadth and Rietveld procedures with the Voigt function. Diffraction data were measured by Bragg–Brentano X-ray diffractometry (XRD), without incident beam monochromatization, and neutron diffractometry (ND) to encompass near-surface and bulk effects, respectively. The specimens consisted of sets of MgO ceramics and MgO–Y_2O_3 ceramic composites sintered over a range of temperatures. An MgO ceramic sintered at 1723 K for 2 h exhibited slightly less XRD broadening than the standard LaB_6 NIST 660 SRM, and was therefore selected to make instrument profile corrections for both XRD and ND data. It was found for both data types that: (*a*) sintering initially relieves residual strain present in the MgO powder used to sinter the ceramics and also promotes grain growth; (*b*) residual strain of the MgO ceramic minimizes as the sintering temperature increases, and then increases with further rise in the sintering temperature, presumably as a result of intragranular interactions associated with grain growth; and (*c*) introduction of the second phase (Y_2O_3) increases strain and inhibits crystal growth. The single-line and Rietveld methods gave similar strain values from both the XRD and ND data within the limits of experimental error, but there were substantial differences between the single-line and Rietveld size estimates determined with the XRD and ND data.

1. Introduction

Strain–size evaluations based on assessments of line profile shape have previously been conducted using various single-line and multi-line procedures and Rietveld-type pattern-fitting approaches (Delhez *et al.*, 1982; Madsen & Hill, 1990; Balzar, 1999). The single- and multi-line methods require careful measurements of the profile shapes and deconvolution of instrument broadening contributions, in either instrument ('real') space or by Fourier inversion.

The Warren–Averbach single-line procedure, involving crystallite strain and size contributions (Warren, 1969), is a popular method in view of the independence of the procedure on the profile function employed. However, two factors limit its reliability, *i.e.* (i) the broadening should be sufficiently large (2–6 times broader than the instrument effects) (Delhez *et al.*, 1980) and (ii) a profile shape 'hook' effect is introduced if the background cannot be determined correctly (Warren, 1969). A 'hook' effect occurs if there are long-tail contributions from the adjacent profiles.

The traditional multi-line Williamson–Hall plot method is unreliable for accurate strain–size evaluations as, in many cases, the results might be physically unacceptable, for example a negative slope (Balzar, 1999) or a negative crystallite size (Balasingh *et al.*, 1991).

The single-line integral-breadth method for strain–size evaluations considered here (designated as the single-line method) has been applied with the Voigt function. The method relies on the assumption that strain contributes only to the Gaussian component of the Voigt function and that the size broadening contributes only to the Lorentzian component (Delhez *et al.*, 1982). It is noted that this assumption has been challenged recently by *e.g.* Wu, Gray & Kisi (1998) and Stephens (1999).

Rietveld-type procedures for strain–size evaluations are based on the refinement of the peak profile shapes. As for the single-line method, the Voigt function has been widely used in Rietveld refinements for strain–size evaluations assuming separate contributions of the Gaussian strain-broadened profile and the Lorentzian size-broadened profile (*e.g.* Madsen & Hill, 1990; Delhez *et al.*, 1993). Recently, progress has been made in strain–size Rietveld modelling by including aniso-

† Currently on leave from the Department of Physics, Institute of Technology 10 November (ITS), Surabaya, Indonesia.

tropic strain effects (*e.g.* Wu, Kisi & Gray, 1998; Stephens, 1999) and by allowing for a size distribution (Langford *et al.*, 2000; Ungár *et al.*, 2001).

This paper summarizes a comparative study of the use of single-line integral-breadth and Rietveld methods for diffraction-broadening strain–size evaluation in MgO materials consisting of an MgO powder, a suite of MgO ceramics produced from the powder, and composite ceramics (with Y_2O_3 as a second phase). Single-line determinations were made with two lines to test the reproducibility of these assessments. The Voigt function was applied for both methods. It is emphasized that the XRD data were recorded without an incident-beam monochromator and therefore that the peak profiles will have been distorted to some extent at low angles. Also, it was not possible to allow for size distribution effects with the Rietveld program employed.

The work forms part of a broader study of strain–size evaluations using physically based strain–size modelling (York, 1999). MgO ceramics were examined for the current study in the expectation that their cubic symmetry might minimize strain and size anisotropy effects. The sintering conditions were varied systematically to provide a range of strain and size effects. XRD and ND were employed to provide near-surface and bulk strain–size assessments, respectively.

A strain–size evaluation requires a standard material with minimum specimen broadening in order to correct for instrumental contributions. In this work, it was found that an MgO ceramic sintered at 1723 K for 2 h showed minimal broadening. While other standards might have been used, such as LaB_6, for this study we employed this MgO ceramic as the standard in order to correct the instrument contributions for both XRD and ND. LaB_6 cannot be used for ND because of severe attenuation effects. Another reason for employing an MgO standard was to perform instrument broadening corrections conveniently at the same Bragg angle as the peak under examination.

2. Methods

2.1. Sample selection and preparation

The raw materials used in the experiment were MgO powder (99% purity, Aldrich Chemicals, USA), containing approximately 10% $Mg(OH)_2$, and Y_2O_3 (Unocal Molycorp, USA). The MgO powder was calcined at 1373 K for 60 min to remove the hydroxide. Two MgO–Y_2O_3 mixtures (10 and 20 wt% Y_2O_3) were prepared for making sintered MgO–Y_2O_3 ceramics. The powders and mixtures were uniaxially pressed at ~38 MPa in a metal die to form cylindrical specimens of diameter 19 mm. The pressed MgO powders were then sintered at temperatures which gave systematic variations in strain and size, *i.e.* at 1373 K for 2 h, 1523 for 2 h, 1723 K for 2 h and 1873 K for 6 h. The pressed MgO–Y_2O_3 mixtures were sintered at 1823 K for 6 h. The final sintered ceramics had diameters ranging from 11 to 19 mm as a result of variations in densification, depending on the sintering temperature.

2.2. Diffraction data collection

X-ray diffraction data were measured using a Siemens D500 Bragg–Brentano instrument, with a Cu tube ($\lambda_{K\alpha_1}$ = 1.54056 Å) operating at 40 kV and 30 mA, an incident-beam divergence slit of 0.3°, a receiving-slit width of 0.15°, a post-diffraction graphite analyser, an NaI detector with pulse discrimination, and specimen rotation. For single-line analysis, the 420 and 422 reflections (2θ = 109.78 and 127.29°, respectively) were measured with a step size of 0.02° and a counting time of 10–12 s step^{-1}. These peaks were selected since the influences of flat specimen and axial divergence are negligible at high 2θ (>90°) when compared with the same effects at low 2θ (Klug & Alexander, 1974). Whole-pattern data for Rietveld analysis were collected over the 2θ range of 20–130° with a step size of 0.02° and a counting time of 2 s step^{-1}.

Neutron diffraction data were acquired with the fixed-wavelength HRPD powder diffractometer at the Australian Nuclear Science and Technology Organization's research reactor HIFAR at Lucas Heights, Australia (Howard *et al.*, 1983). The instrument is configured with 24 He^3 detectors. Specimens of approximately 13 mm diameter and 25 mm height were positioned on a rotating table. The measurement conditions were step size = 0.05°, 2θ range = 5–150°, counting time per step $\simeq$ 13 s and wavelength = 1.493 Å. Corrections for incident-beam fluctuations were made using an incident-beam monitor. The MgO diffraction lines 420 and 422 were found at 2θ = 104.89 and 120.56°, respectively.

2.3. Single-line integral-breadth method

The single-line integral-breadth method for extracting size and strain with the Voigt function was applied according to the procedure proposed by Keijser *et al.* (1982), with profile fitting being carried out with the Voigt function using the *SHADOW* program (Materials Data Inc., 1999). The measured Gaussian and Lorentzian breadths (β_{hG} and β_{hL}, respectively) were used to estimate the specimen-only contributions (β_{fG} and β_{fL}) according to Langford (1978) with the expressions

$$\beta_{fL} = \beta_{hL} - \beta_{gL} \tag{1}$$

and

$$\beta_{fG}^2 = \beta_{hG}^2 - \beta_{gG}^2, \tag{2}$$

where β_{gG} and β_{gL} refer to the instrument-only contributions as measured with a standard displaying minimal broadening.

The angular dependence of β can be analysed to give crystallite size and strain values, assuming that the Gaussian component (β_{fG}) is ascribed to strain and the Lorentzian component (β_{fL}) results from size effects:

$$\beta_{fG} = 4\varepsilon \tan\theta_i, \tag{3}$$

and

$$\beta_{fL} = \lambda / D\cos\theta_i, \tag{4}$$

where ε is the root-mean-square (r.m.s.) crystallite strain, D is the crystallite size estimate and λ is the wavelength.

The standard uncertainties of the integral breadths (β_G and β_L), strain (ε) and crystallite size (D) were estimated with the expressions provided by Keijser *et al.* (1982).

2.4. Rietveld refinement

The Rietveld pattern-fitting procedure allows the refinement of line shape parameters that relate to crystallite strain and size as well as instrument broadening.

Rietveld refinements were performed with the program *Rietica* (Hunter, 1998) which is derived from the Hill–Howard–Hunter *LHPM* program (Hill *et al.*, 1995). The refinement enables the extraction of strain values if the Voigt function is used in which the Gaussian component has the full width at half-maximum (FWHM) H_G as described by Caglioti *et al.* (1958):

$$H_G^2 = U\tan^2\theta + V\tan\theta + W, \tag{5}$$

where U, V and W are refineable parameters. The extraction of the size can be conducted by refining the Lorentzian component (H_L) which is derived from the Scherrer expression

$$H_L = (\lambda/D)\sec\theta, \tag{6}$$

where λ is the wavelength.

The refinements involved the adjustment of the U Voigt peak profile, the 'size parameter' D, lattice parameters, scale factors, background polynomial parameters, 2θ-scale offset and asymmetry (Rietveld, 1969) parameters. The V and W parameters were constrained to the values obtained with the standard by assuming that strain contributes only to the U parameter. The preferred-orientation parameter was not refined. Crystal data for MgO were taken from the Inorganic Crystal Structure Database (FachInformationsZentrum and Gmelin Institute, Germany), ICSD Collection Code 9863, referring to Sasaki & Fujino (1979). Crystal data for Y_2O_3 were taken from the same source (ICSD Collection Code 23811), referring to Paton & Maslen (1965).

The r.m.s. strain, $\varepsilon_{\rm rms}$, can be calculated if the U parameter is refined with the V and W values being fixed at values obtained for the unstrained material, using

$$\varepsilon_{\rm rms} = [(U - U_s)/32\ln 2]^{1/2}, \tag{7}$$

where U and U_s are the parameters obtained from the strained specimen and a strain-free standard, respectively. Equation (7) is derived from expressions provided by Wilson (1963).

Rietica also enables the direct calculation of crystallite size D, if the Voigt function is applied, using the expression

$$D = \lambda/H_L, \tag{8}$$

where H_L is the Lorentzian FWHM and λ is the wavelength. It should be noted that a physical interpretation of the size parameter is likely to have meaning in the case only of ND data for which the instrumental component of the peak shapes is near-Gaussian in form, while for XRD, both Gaussian and Lorentzian components contribute to the instrument broadening (Suortti *et al.*, 1979).

The standard uncertainties for the r.m.s. strain $\varepsilon_{\rm rms}$ and size D were determined by

$$\sigma(\varepsilon_{\rm rms}) = \{[\sigma^2(U) + \sigma^2(U_s)]^{1/2}/(U - U_s)\}(\varepsilon_{\rm rms}/2) \tag{9}$$

and

$$\sigma(D) = [\sigma(H_L)/H_L]D. \tag{10}$$

3. Results and discussion

3.1. Selection of standards for instrument broadening corrections

The FWHM *versus* 2θ plots for the MgO powder and ceramics, for both XRD and ND, are shown in Fig. 1(*a*). It was found for both that the FWHM decreases with sintering temperature, reaching a minimum for the sample sintered at 1723 K for 2 h. The XRD FWHM for the 1873 K–6 h ceramic is substantially higher than that for the 1723 K–2 h ceramic over the 2θ range, whereas the corresponding FWHM values are similar for the ND data. Fig. 1(*b*) compares the FWHM *versus* 2θ plots for MgO ceramic sintered at 1723 K–2 h (0% Y_2O_3) and the composites. As can be seen from this figure, the FWHM for the 0% Y_2O_3 ceramic is substantially less than

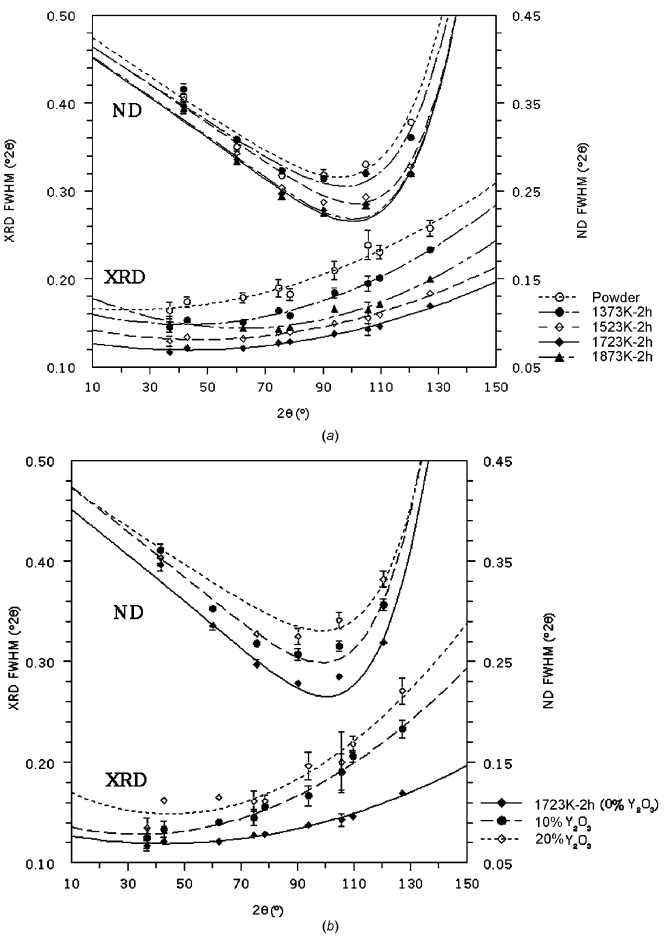

Figure 1
FWHM *versus* 2θ for XRD and ND data. (*a*) MgO powder and MgO ceramics. (*b*) MgO ceramic sintered at 1723 K for 2 h (0% Y_2O_3) and MgO–Y_2O_3 composites. Line fits to the data were made using equation (5).

those of the composites, indicating that the broadening increases with the level of Y_2O_3 addition.

Fig. 2 shows that the XRD FWHM for the MgO ceramic sintered at 1723 K for 2 h is marginally lower than that for the LaB_6 standard reference material (NIST SRM 660 standard; Rasberry, 1989). Accordingly, this MgO material was preferred to SRM 660 for instrument broadening corrections for the XRD analysis. An MgO standard was also developed for the ND strain–size determination as it is clearly valuable to use the same type of material for both XRD and ND strain–size evaluations, and also because LaB_6 cannot be used to correct the ND data because of the severe neutron attenuation. This ND MgO ceramic standard also showed less broadening than the α-Al_2O_3 standard reference material (NIST SRM 676 standard for quantitative analysis; Reed, 1992) for the ND measurements (Fig. 2).

3.2. Line broadening

Fig. 1 clearly indicates that the powder and the composites show substantial broadening. The broadening amounts to only 1.5–2 times that for the 1723 K–2 h ceramic for which there is minimal broadening. The broadening is considerably less than the values typically observed for deformed metals and ultrafine nanocystallites (*e.g.* Klug & Alexander, 1974; Guillou *et al.*, 1995).

The effect of sintering on both the XRD and ND Gaussian and Lorentzian peak breadths is shown in Fig. 3(*a*). It is evident that all four integral-breadth plots decrease with sintering temperature up to 1723 K–2 h, and that further sintering causes broadening of the XRD Gaussian and Lorentzian profile components. A slight increase in the ND Gaussian breadth is also observed, whereas the ND Lorentzian breadth vanishes for the 1723 K–2 h and 1873 K–6 h data sets.

The effects of the sintering on the XRD and ND Rietveld peak shape parameters U [equation (5)] and H_L [equation (6)] is shown in Fig. 3(*b*). Again, it was found that both XRD parameters decrease with sintering temperature up to 1723 K–2 h and then increase at 1873 K–6 h. Similar trends were observed for the ND parameters; however, with less effect at 1873 K–6 h.

These results support the decision made to select the 1723 K–2 h MgO ceramic as the standard for instrument broadening corrections.

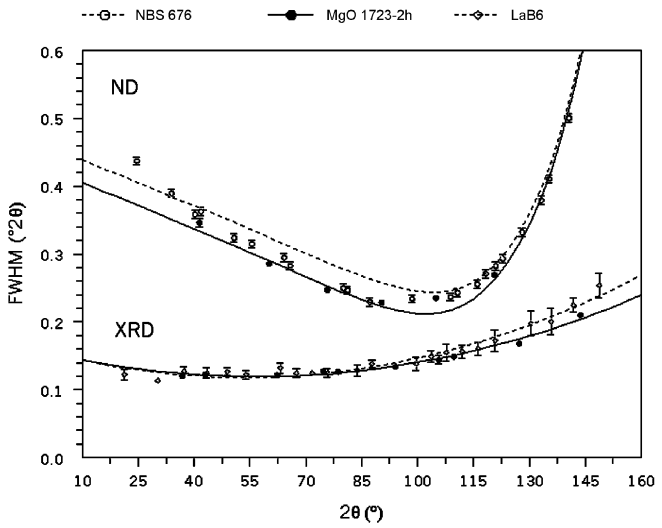

Figure 2
FWHM *versus* 2θ for the MgO ceramic sintered at 1723 K for 2 h. XRD data compared with data for the LaB_6 powder (NIST SRM 660) are represented by the lower curves, while ND data compared with data for the Al_2O_3 powder (NIST SRM 676) are above. Line fits to the data were made using equation (5).

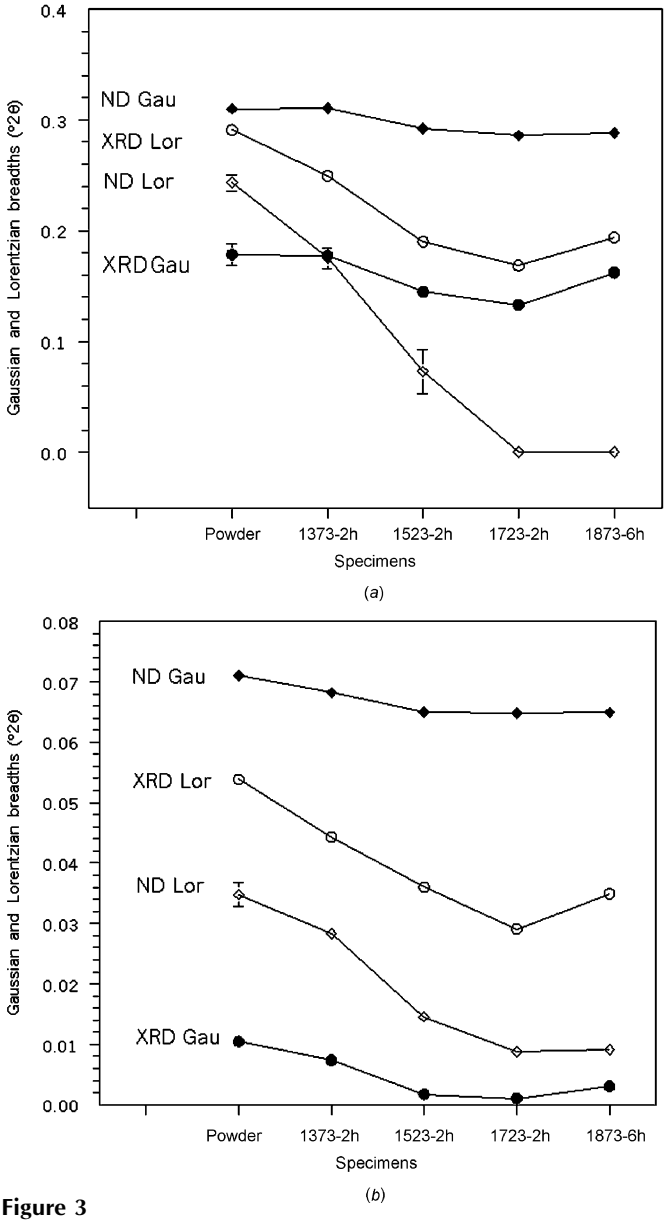

Figure 3
Effects of sintering on the Gaussian and Lorentzian components of the FWHM values for the 422 reflection of the MgO specimens using XRD and ND data: (*a*) from integral breadth analysis; (*b*) from Rietveld analysis. The legend for the horizontal axis denotes the sintering temperature and time (*e.g.* 1373 K for 2 h). Error bars indicate 1 × the standard uncertainty.

3.3. Strain assessments

Fig. 4 (upper panels) shows the XRD and ND strain values for the MgO ceramics as a function of sintering conditions and second-phase content. It is obvious from the XRD single-line and Rietveld methods (left-hand side of upper left panel) that sintering up to 1723 K for 2 h causes strain relief in the near-surface region and further sintering generates additional strain. It appears that intragranular shear interactions associated with grain growth during prolonged sintering increase the strain in the 1873 K–6 h sample. The corresponding ND data (left-hand side of upper right panel), representing strain at depth, are similar to the XRD data with the exceptions that (i) the ND strain for the powder is slightly less than the XRD estimates, and (ii) the enhanced uncertainties for the ND data (attributed to the increased instrumental widths for ND) would mask any increase in ND-derived strain for the 1873 K–6 h sample.

The comparison of the MgO XRD and ND single-line and Rietveld determinations (lower panels of Fig. 4) shows that the (420), (422) and Rietveld results are consistent, and that all (420) and (422) values are reasonably well defined. The ND uncertainties are generally larger than those of XRD, and the Rietveld ND uncertainty estimates become unacceptably large for the ceramics where minimal broadening is observed.

The effect of Y_2O_3 as a second phase on the XRD and ND strain estimates can also be seen in Fig. 4 (right-hand sides of upper panels). It is clear from both the single-line and the Rietveld results that the presence of Y_2O_3 introduces additional strain, which increases with Y_2O_3 content.

The systematic change in strain values with sintering temperature can be explained as follows. At the initial stage of sintering, presumably below 1373 K, the grains start growing and residual internal strains present as a result of powder processing are reduced. When the sintering process is completed, the grain size has become larger than the initial powder size, the porosity is minimal and the residual strain is also minimal. If additional heat treatment is applied, the grains will grow further. However, with the absence of porosity, the

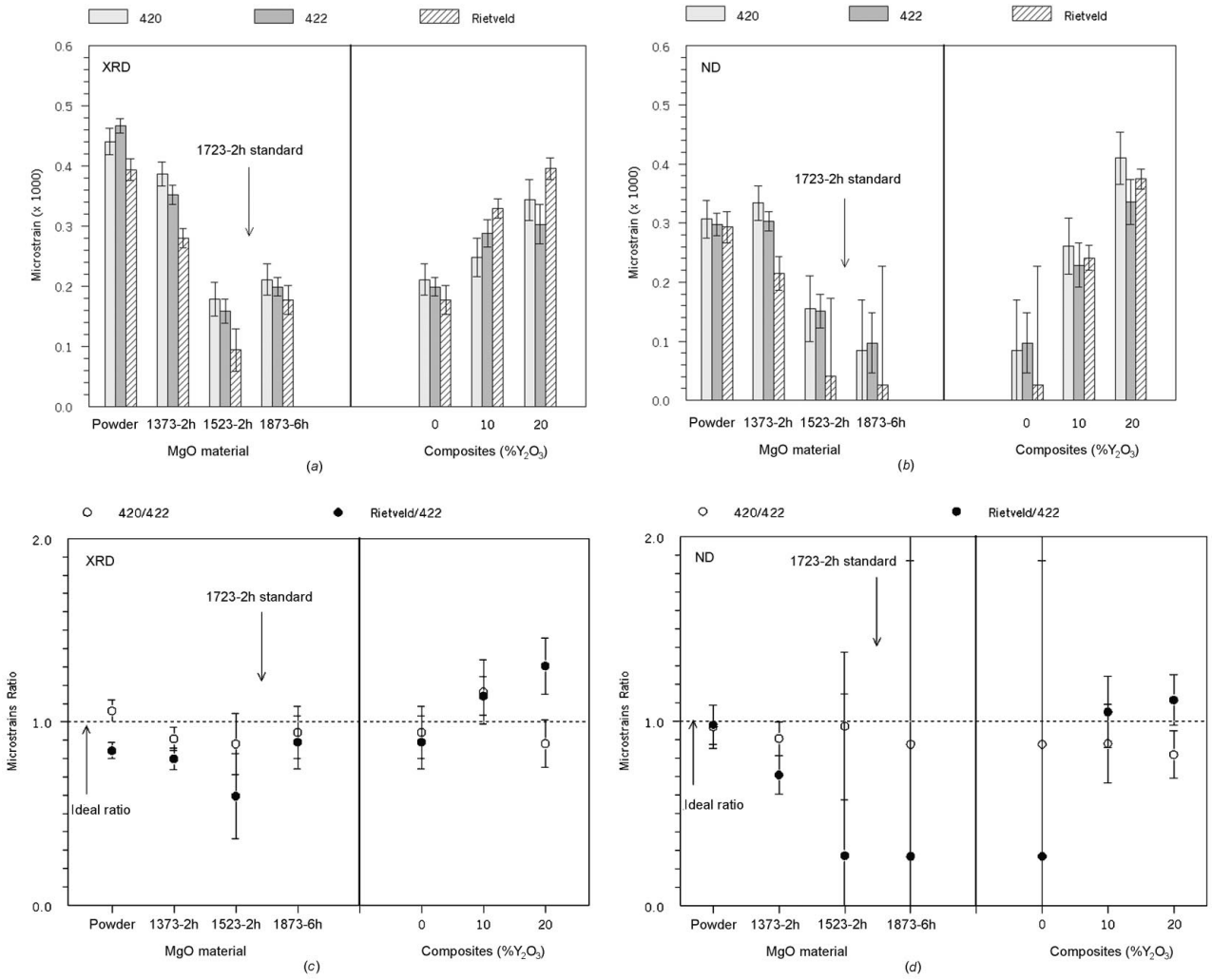

Figure 4
Microstrain values *versus* sintering temperature and Y_2O_3 content obtained from XRD data (top left) and ND data (top right). The composites were sintered at 1823 K for 6 h. The data labelled 0% Y_2O_3 are the same as the 1873 K–6 h MgO data. The lower diagrams give the corresponding ratios of microstrain values for the 420 and 422 single-line estimates (left) and the Rietveld and 422 single-line microstrain values (right). Error bars indicate 1 × standard uncertainty; error bars for the 1523–2 h and 1873 K–6 h ND microstrain values are off the scale.

grains will tend to undergo further interactions causing shear strains. This process will develop non-uniform strains, as shown by the increase in Gaussian broadening.

3.4. Size assessments

The single-line size estimates show that sintering favours crystallite growth in the pure MgO specimens (Fig. 5). The Rietveld results give the same trend, but with significantly smaller size values for the XRD analysis and larger values for the ND data. The single-line XRD estimates for the 1523 K–2 h ceramic agree well with scanning electron microscopy (SEM) surface measurements of grain size, which show a range of 800–1700 nm, with a mean value of 1400 nm. The corresponding single-line XRD estimates are approximately 1000 nm, whereas the Rietveld estimate is 250 nm. Further, the single-line size estimates seem to be more reasonable in that constraints on grain growth for the bulk (ND results) should be more substantial than might apply to the near-surface (XRD). The generally higher Rietveld size estimates found from the ND data, relative to XRD, appear to be unreasonable.

Single-line size estimates could not be made for the ND 1873 K–6 h data (Fig. 5) as the Lorentzian breadths for this specimen and for the 1523 K–2 h sample were the same within experimental limits (see Fig. 3).

Fig. 5 also indicates that for both methods the presence of Y_2O_3 as a second phase inhibits crystallite growth. The single-line method shows that the estimated crystallite size for MgO in the composites is similar to that for the powder. The Rietveld size decreases with the level of Y_2O_3 addition, and the Rietveld sizes are consistently larger than the single-line sizes. The role of a second phase in constraining grain growth in ceramic materials is widely known (Kingery *et al.*, 1976). For example, ZrO_2 inhibits grain growth in Al_2O_3 ceramics (Lange & Hirlinger, 1984).

It appears that the model for crystallite size determination by the Rietveld method gives inconsistent results. Presumably,

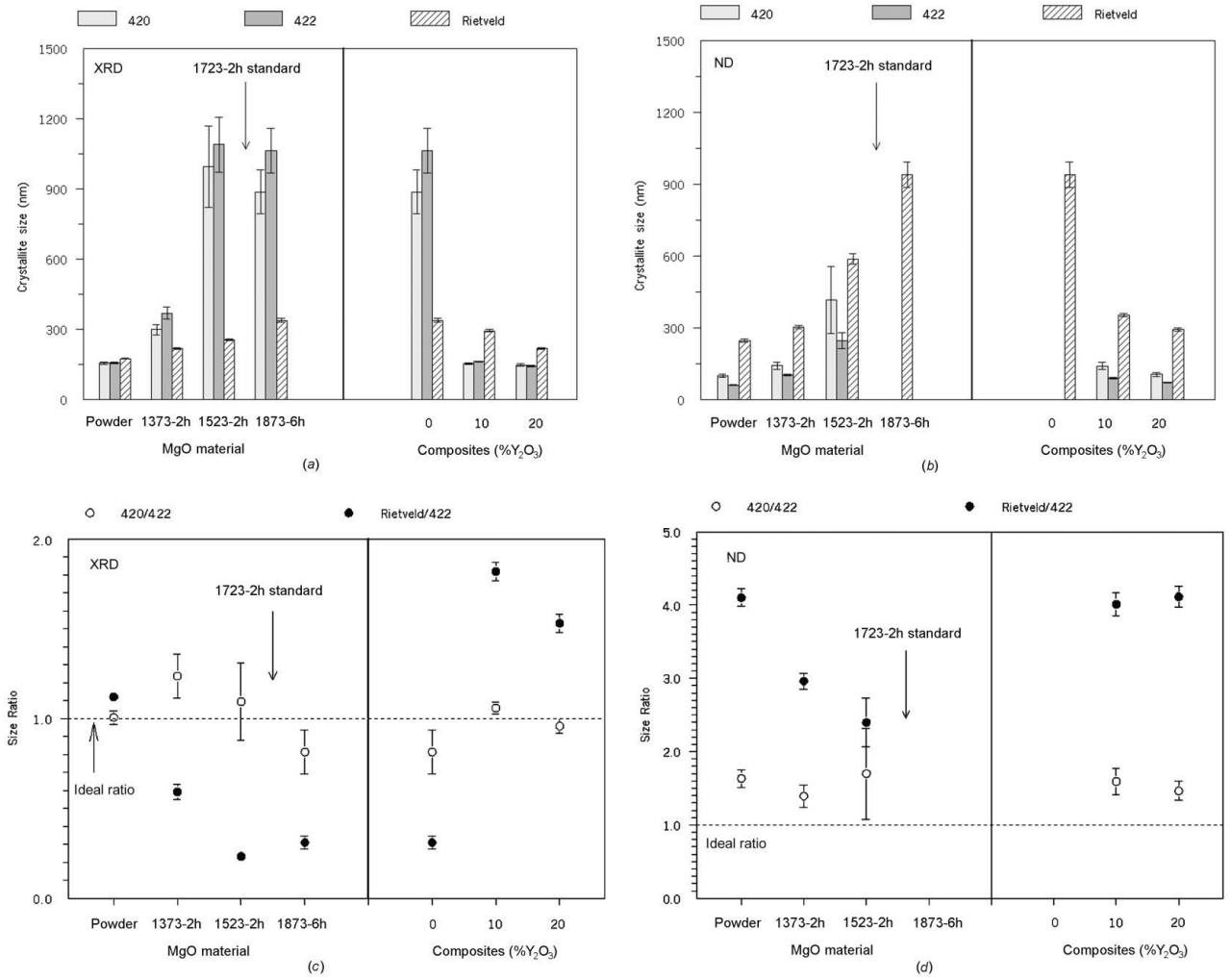

Figure 5
Size values *versus* sintering temperature and Y_2O_3 content obtained from XRD data (top left) and ND data (top right). The single-line ND crystallite size for the 1873 K–6 h sample cannot be determined as the associated Lorentzian components are zero (see Fig. 3*a*). The composites were sintered at 1823 K for 6 h. The lower diagrams give the corresponding ratios of strain values for the 420 and 422 single-line estimates (left) and the Rietveld and 422 single-line size values (right). Error bars indicate 1 × standard uncertainty.

this arises from the model for the instrument profile, which in both XRD and ND is assumed to be Voigtian. The ND peak shape for the standard specimen is very close to Gaussian, as observed by others (*e.g.* Suortti *et al.*, 1979; Albinati & Willis, 1982), while the instrument profile model for XRD is more complicated (Klug & Alexander, 1974; Suortti *et al.*, 1979). It should also be noted that the Voigt function adopted for this line profile analysis does not take into account the existence of a particle size distribution, rather than a monosize microstructure which may lead to the extraction of dubious size values.

3.5. Quality of the Rietveld assessments

The strain–size assessments made using the Rietveld method are less consistent than those made using the single-line method. The results obtained from XRD and ND data for the MgO ceramics show that the Rietveld-derived strain differs appreciably from the single-line determinations with, in general, inferior precision. It is also found that the Rietveld size values disagree with the single-line sizes.

Despite the possibility of acquiring strain–size information using the Voigt function, it should be emphasized that the Gaussian strain and Lorentzian size assumptions have no direct physical basis. It is therefore of value to model each effect following considerations that have direct microstructural interpretation. York (1999) has derived analytical profile functions with parameters that are directly correlated to crystallite size distribution, average crystallite size and strain distribution. Work is now in progress to implement and improve the York model for strain–size evaluation with particular emphasis on sintered ceramic materials.

3.6. Near-surface and bulk strain evaluations

The similarity of the strain values obtained by XRD and ND for the ceramics and composites indicates that both the near-surface and the bulk exhibit similar shear-strain (or non-uniform microstrain) behaviour. It is well known that when a ceramic material is cooled during sintering, differences in contraction behaviour between the surface and the bulk might cause tensile and compressive stresses, respectively (Kingery *et al.*, 1976). This behaviour, however, appears not to be correlated with the non-uniform microstrain. It is expected that this behaviour is associated with the uniform microstrain, which can be determined by assessing the diffraction line shifts.

Differences between the XRD and ND size values for the ceramics and the composites might be caused by differences either in the average near-surface and bulk grain sizes or in the near-surface and bulk crystallite size distributions. The latter cannot be deduced from this study as it is not taken into account by the Voigt function.

4. Conclusions

The results obtained by both the single-line and Rietveld methods using the Voigt function applied to XRD and ND data showed that sintering relieves residual strain and induces crystallite growth in MgO ceramics. In addition, the introduction of Y_2O_3 as a second phase increases the strain and constrains crystallite growth. Both methods also show that further sintering in pure MgO develops strain, which is presumably caused by the shear interactions between neighbouring grains.

Generally, consistent strain values are obtained by the single-line and Rietveld methods using both XRD and ND data, whereas there are marked differences between the size estimates obtained by the two methods. The inconsistency of the results indicates that profile functions involving parameters representing the crystallite size distribution and anisotropic strain should be developed.

The methods have shown the reliability of the MgO ceramic as a standard for line broadening analysis.

The authors acknowledge the Australian Agency for International Development (AusAID) for awarding a PhD scholarship to SP, and the Australian Institute of Nuclear Science and Engineering (AINSE), grant numbers 00/119P and 01/112, for funding the ND data measurements.

References

Albinati, A. & Willis, B. T. M. (1982). *J. Appl. Cryst.* **15**, 361–374.
Balasingh, C., Abuhasan, A. & Predecki, P. K. (1991). *Powder Diffr.* **6**, 16–19.
Balzar, D. (1999). In *Defect and Microstructure Analysis by Diffraction*, edited by R. Snyder, J. Fiala & H. J. Bunge, pp. 94–126. IUCr/Oxford University Press.
Caglioti, G., Paoletti, A. & Ricci, F. P. (1958). *Nucl. Instrum.* **3**, 223–228.
Delhez, R., de Keijser, Th. H., Langford, I. J., Louër, D., Mittemeijer, E. J. & Sonneveld, E. J. (1993). *The Rietveld Method*, edited by R. A. Young, pp. 132–166. IUCr/Oxford University Press.
Delhez, R., de Keijser, Th. H. & Mittemeijer, E. J. (1980). *Accuracy in Powder Diffraction*, *National Bureau of Standards Special Publication No. 567*, edited by S. Block & C. R. Hubbard, pp. 213–253. Washington, DC: National Bureau of Standards.
Delhez, R., de Keijser, Th. H. & Mittemeijer, E. J. (1982). *Fresenius Z. Anal. Chem.* **312**, 1–16.
Guillou, N., Auffrédic, J. P. & Louër, D. (1995). *Powder Diffr.* **10**, 236–240.
Hill, R. J., Howard, C. J. & Hunter, B. A. (1995). Australian Atomic Energy Commission (now ANSTO) Report No. M112, Lucas Heights Research Laboratories, New South Wales, Australia.
Howard, C. J., Ball, C. J., Davis, R. L. & Elcombe, M. M. (1983). *Aust. J. Phys.* **36**, 507–518.
Hunter, B. A. (1998). *International Union of Crystallography, Commission on Powder Diffraction – Newsletter*, 20, 21.
Keijser, Th. H. de, Langford, J. I., Mittemeijer, E. J. & Vogels, A. B. P. (1982). *J. Appl. Cryst.* **15**, 308–314.
Kingery, W. D., Bowen, H. K. & Uhlmann, D. R. (1976). *Introduction to Ceramics*, 2nd ed., pp. 448–515. New York: John Wiley.
Klug, H. P. & Alexander, L. E. (1974). *X-ray Diffraction Procedures for Polycrystalline and Amorphous Materials*, 2nd ed., pp. 271–418, 619–708. New York: Wiley.
Lange, F. F. & Hirlinger, M. M. (1984). *J. Am. Ceram. Soc.* **67**, 164–168.
Langford, J. I. (1978). *J. Appl. Cryst.* **11**, 10–14.
Langford, J. I., Louër, D. & Scardi, P. (2000). *J. Appl. Cryst.* **33**, 964–974.

Madsen, I. C. & Hill, R. J. (1990). *Powder Diffr.* **5**, 195–199.
Materials Data Inc. (1999). *SHADOW, Phase Fitting*. Version 4.2. Materials Data Inc., Livermore, CA, USA.
Paton, M. G. & Maslen, E. N. (1965). *Acta Cryst.* **19**, 307–310.
Rasberry, S. D. (1989). *Certificate of Analysis, Standard Reference Material 660. Instrument Line Position and Profile Shape Standard for X-ray Powder Diffraction.* National Institute of Standards and Technology, Gaithersburg, MD, USA.
Reed, W. P. (1992). *Certificate of Analysis, Standard Reference Material 676. Alumina Internal Standard for Quantitative Analysis by X-ray Powder Diffraction.* National Institute of Standards and Technology, Gaithersburg, MD. USA.
Rietveld, H. M. (1969). *J. Appl. Cryst.* **2**, 65–71.
Sasaki, S., Fujino, K. & Takeuchi, Y. (1979). *Proc. Jpn Acad.* **55**, 43–48.
Stephens, P. W. (1999). *J. Appl. Cryst.* **32**, 281–289.
Suortti, P., Ahtee, M. & Unonius, L. (1979). *J. Appl. Cryst.* **12**, 365–369.
Ungár, T., Gubicza, J., Ribarik, G. & Borbely, A. (2001). *J. Appl. Cryst.* **34**, 298–310.
Warren, B. E. (1969). *X-ray Diffraction.* Reading, Mass: Addison Wesley.
Wilson, A. J. C. (1963). *Proc. Phys. Soc. London*, **81**, 41–46.
Wu, E., Gray, E. A. & Kisi, E. H. (1998). *J. Appl. Cryst.* **31**, 356–362.
Wu, E., Kisi, E. H. & Gray, E. A. (1998). *J. Appl. Cryst.* **31**, 363–368.
York, B. R. (1999). *Adv. X-ray Anal.* **41**, 544–555.